Highly Excited Bound and Low-Lying Resonance States of H_2O[†]

Stephen K. Gray*

Chemistry Division, Argonne National Laboratory, Argonne, Illinois 60439

Evelyn M. Goldfield[‡]

Chemistry Department, Wayne State University, Detroit, Michigan 48202

Received: October 17, 2000; In Final Form: December 12, 2000

A theoretical study of the highest bound states and some of the lowest energy resonance states of water in its ground electronic state, $\tilde{X} = 1^1A'$, and with zero total angular momentum, is presented. The majority of our calculations correspond to the even symmetry block with respect to hydrogen atom exchange. An accurate ab initio based potential surface is employed. The Lanczos method, applied to a large grid representation of the Hamiltonian, is shown to be a straightforward method for obtaining the bound state energy levels. Selected eigenfunctions are also determined and several of those near the dissociation threshold are quite extended. Resonance states just above the dissociation threshold are characterized with the aid of damped Chebyshev iterations. Among the resonances observed are those with hyperspherical and local mode character.

I. Introduction

The ground electronic state of water, $H_2O(\tilde{X}=1^1A')$, is of fundamental interest. Experiments can now access highly vibrationally excited states of water,[1] and the low-lying resonance states may also prove to be accessible.[2] Potential energy surfaces based on high-quality ab initio data[3,4] are also available. Theoretical methods for the determination of vibration−rotation states are now sufficiently advanced that it is possible to calculate many highly excited states of water.[4−9] We present the results of detailed theoretical calculations on the nature of the bound and resonance states of water near the OH + H threshold that we hope will motivate both future theoretical and theoretical work.

Two iterative techniques, the Lanczos method[10,11] for the bound states and damped Chebyshev iterations[12−15] for the resonance states, are applied to the accurate, ab initio based H_2O potential surface of Ho et al.[3] Mussa and Tennyson[5,6] previously presented an impressive quantum study of many rovibrational states employing the same potential surface. Another related work on water is a detailed study of 2D and 3D bound and resonance states, employing an empirical potential surface, by Hartke et al.[16] By converging and analyzing the highest bound states and low-lying resonances, our work complements and extends this earlier work.

Section II outlines our methods and computational details, section III discusses the bound and resonance state results, and section IV concludes.

II. Methods

The problems of determining bound and resonance states involve similar considerations. One must decide on the representation, i.e., what coordinate system and basis set or grids are to be employed. One must also decide on the actual method of determining the relevant properties (e.g., eigenvalues) of the Hamiltonian operator in the representation. There are numerous theoretical approaches to obtaining excited ro-vibrational states.[5,8,9,17] One approach, as in the work of Carrington and co-workers,[8,9] is to use relatively primitive and large grid or discrete variable representations (DVRs),[18] coupled with an iterative matrix eigenvalue method such as the Lanczos method.[10,11] This primitive grid approach can, by its egalitarian nature regarding the problem representation, describe states that are extremely exited and distorted. However the matrices involved are large and hence the need of an iterative matrix eigenvalue method. A recent comparative study of bound state methods in relation to determining all the vibrational states of HOCl confirms this point.[19] (See also the interesting comparative study in ref 9.) Such approaches can require additional effort or more sophisticated considerations to obtain eigenfunctions. See refs 20−22 for some interesting recent developments on inferring eigenstate information as well. Section IIA outlines our basic representation of the problem which is common to both our bound state and resonance work, section IIB outlines how the bound states were determined (Lanczos method), and section IIC outlines how the resonance states were determined (damped Chebyshev iterations).

A. Representation. We performed bound state (Lanczos) calculations within both Jacobi and Radau coordinate[5,7,23] representations. Within each representation we considered a variety of grid and basis set sizes. Jacobi and Radau coordinates lead to very similar $J = 0$ three-atom Hamiltonians. The Jacobi coordinates employed are R, r, and γ, where R is the distance from O to the H_2 center of mass, r is the H_2 internuclear distance, and γ is the angle between the vectors associated with R and r. Radau coordinates involve two distances R_1 and R_2 and an angle α that can be taken to be similar to (but not exactly the same as) the two OH bond distances and associated bending angle.[23] One expects a Radau coordinates representation would be more computationally efficient (e.g., require smaller Hamiltonian matrices) for describing *most* of the vibrational states of water. The *highest* energy bound states and the resonance states,

[†] Part of the special issue "William H. Miller Festschrift".

* Corresponding author. E-mail: gray@tcg.anl.gov.
[‡] E-mail: evi@sun.science.wayne.edu.

10.1021/jp003821z CCC: $20.00
Published on Web 02/01/2001

TABLE 1: Grid[a] and Related Details

	Bound State Calculations		
	Jacobi Coordinates (R, r, γ)		
J-1	$R^{min} = 0$ a$_0$ $r^{min} = 0.5$ a$_0$ $j = 0, 2, ..., 78$ (40 even exchange symmetry Legendre polynomials in cos γ)	$R^{max} = 12.5$ a$_0$ $r^{max} = 13.5$ a$_0$	$N_R = 179$ $N_r = 179$
J-2:	$R^{min} = 0$ a$_0$ $r^{min} = 0.5$ a$_0$ $j = 0, 2, ..., 98$ (50 even exchange symmetry Legendre polynomials in cos γ)	$R^{max} = 14.5$ a$_0$ $r^{max} = 15.5$ a$_0$	$N_R = 209$ $N_r = 209$
J-3:	$R^{min} = 0$ a$_0$ $r^{min} = 0.5$ a$_0$ $j = 0, 2, ..., 118$ (60 even exchange symmetry Legendre polynomials in cos γ)	$R^{max} = 17.8$ a$_0$ $r^{max} = 19.0$ a$_0$	$N_R = 255$ $N_r = 255$
	Radau Coordinates (R_1, R_2, α)		
R-1:	$R_i^{min} = 0.5$ a$_0$ $j = 0, 1, ..., 79$ (80 Legendre polynomials in cos α)	$R_i^{max} = 12$ a$_0$	$N_i = 179$
	Resonance State Calculations[b]		
J-4:	$R^{min} = 0$ a$_0$ $r^{min} = 0.5$ a$_0$ $j = 0, 2, ..., 78$ (40 even exchange symmetry Legendre polynomials in cos γ)	$R^{max} = 14.58333$ a$_0$ $r^{max} = 15.66666$ a$_0$	$N_R = 209$ $N_r = 209$

[a] Each grid corresponds to $x_i = x^{min} + k\Delta x$, $\Delta x = (x^{max} - x^{min})/(N_x + 1)$, $x = R$ or r. The potential and centrifugal terms in the Hamiltonian in all calculations are also cut off at 0.44 au (96 569 cm^{-1}) relative to the bottom of the potential well. [b] Absorption: $A(r) = \exp[-C_a(r - r_a)^2]$, $r > r_a$ and $A(r) = 1$ otherwise, $C_a = 0.005$ a$_0^{-2}$, $r_a = 10$ a$_0$.

however, can be either very extended and/or mixed in character. Thus, any representation used to obtain these states will involve large, dense grids. We found that in this limit the Radau system is not significantly more advantageous than the Jacobi one. Jacobi coordinates also allow one to easily impose even or odd exchange symmetry with respect to the hydrogen atoms. (One may also impose symmetry with grids based on symmetrized Radau coordinates.)[5,7] The resonance state (damped Chebyshev) calculations were carried out in Jacobi coordinates.

Both iterative approaches used (sections IIB and IIC) require repeated evaluations of $\mathbf{H}\cdot\mathbf{q}$, where $\mathbf{q}$ is a real vector and $\mathbf{H}$ is the corresponding Hamiltonian matrix representation. As in previous work,[15] the Jacobi representation is based on evenly spaced grids in R and r, and a (normalized) Legendre basis, $P_j(\cos\gamma)$. The components of the vector $\mathbf{q}$ are thus indexed by i_R, i_r, and j, denoting the specific R, r grid point and the jth Legendre polynomial. Even or odd hydrogen exchange symmetry corresponds to including only even or odd Legendre polynomials in the basis. Cutoff energies are applied to both the potential and centrifugal terms of the Hamiltonian.[15] Fast Fourier sine transforms are used to evaluate the R and r kinetic energy terms, and the effect of the potential on a vector is evaluated via transformation to the corresponding cos(γ) grid representation, multiplication by the potential points on the grid, and back transformation to the Legendre representation.[15] The bound state calculations carried out with the Radau coordinate representation involved an almost identical treatment of the evaluation of $\mathbf{H}\cdot\mathbf{q}$. See Table 1 for the details of several grid and basis set choices we have explored.

B. Lanczos Method for the Bound States. The Lanczos method[10,11] involves application of the following three-term recursion to generate the various Krylov vectors $\{\mathbf{q}_k\}$

$$\beta_k\mathbf{q}_{k+1} = -\beta_{k-1}\mathbf{q}_{k-1} + (\mathbf{H} - \mathbf{I}\alpha_k)\cdot\mathbf{q}_k, \quad k = 1, 2, ..., M \qquad (1)$$

where $\mathbf{I}$ is the identity matrix. Equation 1 is initiated with an arbitrary, normalized $\mathbf{q}_1$ and $\beta_0 \equiv 0$. The real numbers $\alpha_k = \langle\mathbf{q}_k|\mathbf{H}|\mathbf{q}_k\rangle$ and $\beta_k = \langle\mathbf{q}_k|\mathbf{H}|\mathbf{q}_{k-1}\rangle$ are generated during the course of the iterations in an economical manner involving no additional matrix-vector products. At any stage M, one can form a tridiagonal matrix $\mathbf{T}$ with the α_k as diagonal elements and the β_k as the nonzero off-diagonal elements. Diagonalization of $\mathbf{T}$ yields estimates of the eigenvalues of $\mathbf{H}$. In exact arithmetic, the Krylov vectors generated via eq 1 are orthonormal but in practice round-off errors destroy this property. This much-discussed aspect of the Lanczos method leads to complications, e.g., multiple copies of good eigenvalues and spurious or ghost eigenvalues. Nonetheless, as discussed by Cullum and Willoughby,[10] one may apply checks on the eigenvalues of $\mathbf{T}$ to filter out the incorrect eigenvalues. In this work, we used the conceptually simpler procedure of comparing sets of eigenvalues obtained at stage M with one or more previous sets generated at stages $M' < M$. (This procedure was also used in a determination of all the bound states of HOCl.)[19]

If $\mathbf{c}^n$ is an eigenvector of the $\mathbf{T}$ corresponding to some good eigenvalue of $\mathbf{H}$, E_n, the corresponding eigenvector $\mathbf{v}^n$ of $\mathbf{H}$ can be approximated by

$$\mathbf{v}^n \approx N\sum_{k=1} c_k{}^n\mathbf{q}_k \qquad (2)$$

where N is a normalization constant such that $\langle\mathbf{v}^n|\mathbf{v}^n\rangle = 1$. It is interesting to note that if $c_1{}^n = 1$, then a scalar form of eq 1, with the $\mathbf{q}_k$ replaced by $c_k{}^n$ and $\mathbf{H}$ replaced by E_n, can be used to generate the $c_k{}^n$ in eq 2. See also ref 20 for a related, but different approach. Unfortunately, for large problems such as the present one, it is not practical to keep all the $\mathbf{q}_k$ in memory, or even to store them all on external disk. If eigenvectors are desired, an additional Lanczos calculation is therefore required to regenerate the $\mathbf{q}_k$ and to construct one or more selected eigenstates according to eq 2. (If many eigenvectors are desired, more than one extra Lanczos calculation might be needed since it may not be possible to store simultaneously many different $\mathbf{v}^n$.) The loss of orthogonality of the Krylov vectors during the course of the Lanczos iterations leads to some interesting properties of the approximate eigenvectors given by eq 2. For

example, if one considers the standard deviation

$$\sigma^n = (\langle \mathbf{v}^n|\mathbf{H}^2|\mathbf{v}^n\rangle - \langle \mathbf{v}^n|\mathbf{H}|\mathbf{v}^n\rangle^2)^{1/2} \quad (3)$$

one finds that it does not uniformly decrease as the number of Lanczos iterations M is increased. Rather, σ^n oscillates and the best strategy is to monitor σ^n as one forms $\mathbf{v}^n$ and to simply always save the $\mathbf{v}^n$ that leads to the smallest σ^n over the course of the iterations. This procedure worked very well for the present purposes. In addition, the states obtained were verified to be orthogonal to between 4 and 9 significant figures, which further confirms the overall procedure. [Note that in order to visualize a wave function consistent with a given $\mathbf{v}^n$, one must construct $\psi^n(R_{i_R},r_{i_r},\cos\,\gamma) = \sum_j v^n{}_{i_R,i_r,j}\,\bar{P}_j(\cos\,\gamma)$.]

Typically, about 40 000 Lanczos iterations were required to converge *all* the bound states, which for the largest grid and basis set considered (dimension $\approx 3.9 \times 10^6$) required nearly 2 days of computation time on a 667 MHz Compaq XP1000 (Dec-Alpha) workstation. (While obviously computationally intensive, the programming of the approach is extremely straightforward.)

C. Damped Chebyshev Iterations for the Resonance States. Resonances correspond to complex energies $E_n - i\Gamma_n/2$ of the Hamiltonian, where outgoing boundary conditions have also been enforced. To find these complex energies, one could augment **H** by an optical potential and employ stabilization ideas.[24−26] Another approach, which is essentially what we employ here, is a spectral approach based on wave packet propagation. Assuming that the effect of dissociation on interaction region dynamics is appropriately mimicked by absorbing outgoing wave packet components, spectral analysis of a correlation function can be used to obtain resonance properties.[27,28] The main idea is that a correlation function inferred from a time-evolving wave packet will then exhibit damped oscillations, with the oscillation frequencies being related to resonance energy positions, and the damping factors being related to the resonance decay widths.[27,28] The approach used here, based on Mandelshtam and Taylor's damped Chebyshev iteration,[12−15] is in this latter spirit.

If $\mathbf{H}_S = a_S\mathbf{H} + b_S$, with a_S and b_S being chosen to ensure that the eigenvalues of $\mathbf{H}_S$ lie within $[-1, 1]$, a damped Chebyshev iteration[12−15] can be defined as

$$\mathbf{q}_{k+1} = \mathbf{A}\cdot[-\mathbf{A}\cdot\mathbf{q}_{k-1} + 2\mathbf{H}_S\cdot\mathbf{q}_k], \quad k = 1, 2, ... \quad (4)$$

where the role of **A** is to damp away outgoing components of the iterates, $\mathbf{q}_k$, corresponding to amplitude growth in the dissociation region, thus allowing one to model the effective dynamics in the interaction region. Given some $\mathbf{q}_1$, one sets $\mathbf{q}_2 = \mathbf{A}\cdot\mathbf{H}_S\cdot\mathbf{q}_1$ and applies eq 4 to generate the subsequent vectors. The damping matrix **A** is diagonal with respect to a grid point representation, with positive real diagonal elements that are unity in the interaction region and less than unity outside the interaction region in order to absorb outgoing products and prevent artificial reflection effects. **A** effectively accomplishes what an (imaginary) optical or absorbing potential[24,25] would accomplish but is real valued. Thus, if **H** is real (as it is in the present and many other applications), eq 4 involves only real objects.

Mandelshtam and Taylor introduced this approach, and coupled it with filter diagonalization (FD)[29] ideas to obtain a useful method for obtaining resonance positions and decay widths.[12−14] Equation 4 can also be interpreted as being a rule for generating the real part, **q**, of a wave packet at time $t = (k + 1)\tau$, given knowledge of its real parts at times $(k - 1)\tau$ and $k\tau$, where the underlying Hamiltonian operator that generates the wave packet is not simply **H** or $\mathbf{H}_S$ but[15]

$$f(\mathbf{H}_S) = -\frac{\hbar}{\tau}\cos^{-1}\mathbf{H}_S \quad (5)$$

and τ is an arbitrary time step that cancels out of any expression for an observable. If the various iterates $\mathbf{q}_k$, $k = 1, 2, ...$, consistent with eq 4, are dominated by resonances, then the autocorrelation function $C(t{=}k\tau) = \langle \mathbf{q}_0|\mathbf{q}_k\rangle$ will be a superposition of L damped oscillatory terms

$$C(t{=}k\tau) = \sum_{j=1}^{L} h_j \cos(\theta_j k)\exp(-\gamma_j k/2) \quad (6)$$

(In practice, L values larger than the number of resonances present are usually used in order to describe background or direct features.) When damping is applied to the dynamics, this behavior is consistent with the eigenvalues f_n of $f(\mathbf{H}_S)$ being complex numbers:

$$f_n = \frac{\hbar}{\tau}\left(\theta_n - i\frac{\gamma_n}{2}\right) \quad (7)$$

where $\gamma_n \geq 0$. By taking the cosine of eq 7 one may relate the parameters θ_n and γ_n to the actual resonance position and width of the original Hamiltonian:

$$E_n = \frac{1}{a_S}[\cos(\theta_n)\cosh(\gamma_n/2) - b_S]$$

$$\Gamma_n = \frac{\sin(|\theta_n|)\sinh(\gamma_n/2)}{a_S} \quad (8)$$

If one has a reasonable (not necessarily exact) estimate of the energy, E_n, of some resonance, it is possible to obtain a good idea of the resonance wave function by constructing

$$\mathbf{r}^n = N\sum_{k=1} \cos(\theta_n k)\mathbf{q}_k \quad (9)$$

where the sum is over all the Chebyshev iterations.

This spectral approach involves inferring the resonance parameters in eq 6, given a sequence of correlation function points. An explicit discrete Fourier transform is the best way of inferring the parameters, but, depending on the duration of the correlation function sample, the uncertainties associated with the parameters can be large. An alternative is to treat eq 6 as a nonlinear fitting problem. We use the Prony method[30] to accomplish the required fits, in a manner similar to that outlined in the Appendix of ref 28.

If one assumes that the $\mathbf{q}_k$ can be expanded in terms of a set of orthogonal oscillatory, decaying resonance states in k, then it is easy to show that $2\langle \mathbf{q}_k|\mathbf{q}_k\rangle = C(t{=}2k\tau) + f(k)$, where $f(k)$ corresponds to a sum of decaying exponentials. This implies that, apart from an extra $\theta = 0$ term in eq 6, $2\langle \mathbf{q}_k|\mathbf{q}_k\rangle$ and $C(t{=}2k\tau)$ have the same Fourier decompositions; i.e., one can infer correlation function information corresponding to $2k$ iterations from the result at k iterations. This is similar in spirit to a related trick in ordinary wave packet dynamics.[31] (It is, however, not as general as the ordinary wave packet dynamics trick.) Therefore spectral analysis of $2\langle \mathbf{q}_k|\mathbf{q}_k\rangle$, as opposed to $C(t{=}k\tau) = \langle \mathbf{q}_0|\mathbf{q}_k\rangle$, can lead to significantly better resolution.

If only a relatively small number of resonances are of interest, we find it useful to employ initial conditions that target the desired resonances.[28] The bound state Lanczos calculations automatically provide good initial conditions for targeting the

resonance states: it is possible to converge many energy levels above the dissociation threshold, and to determine the corresponding "eigenstates" as already described in section IIB. Of course, these are only eigenstates in relation to the finite grid and basis set representation employed. (Such states and their variation with grid or box size are used in stabilization approaches to resonances.)[24−26] If subsequently propagated on a grid that includes absorption of outgoing components, these states will decay.

In many instances we propagated individual Lanczos-based eigenstates. Another approach is to construct a superposition of Lanczos states with energies in a desired region. Some care is required in constructing the superposition because sometimes there are resonance interactions such that the sum of two energetically close Lanczos states leads to an object without localization in the main interaction region. (See also the discussion of the bound state results in section IIIA.) To minimize this effect, we consider the overlap of a given Lanczos state with its lower energy nearest-neighbor within the interaction region, e.g., the overlap is evaluated only over OH bond distances less than 6 a_0. (Of course the overlap over the entire configuration space should be zero or, with our numerical eigenstates, almost zero.) If this overlap is negative, then the current Lanczos state is multiplied by -1 before being added to the superposition to avoid cancellation of amplitude in the interaction region. This approach allows construction of a superposition state with significant amplitude in the interaction region and reasonable intensity in the most important resonance states. Of course, this phase convention may then lead to superposition states with relatively little weighting associated with very short-lived resonances that have signficant amplitude in the extended regions of configuration space. Other superpositions with different phases can be considered. As a consistency check, the information obtained in a superposition propagation must, of course, be consistent with or complement the results of various individual state propagations.

A summary of our overall approach to obtaining resonance information may be useful. First, a (grid) representation of the Hamiltonian operator, similar to that employed in the bound state calculations, is adopted (section IIA). Suitable initial vectors are chosen, based on the bound state calculations, that we believe contain appreciable resonance character. The initial conditions are iterated (or propagated) according to eq 4, the damped Chebyshev iteration,[14] which is very similar in spirit to propagating a wave packet in time as discussed above and elsewhere.[15] The autocorrelation function is formed from the iterates and analyzed with the Prony method to obtain the resonance positions and decay widths.[28] If actual resonance wave functions are also desired, additional propagations involving a Fourier transformation, eq 9, of the evolving vector iterates must be carried out. There are clear parallels with iterative matrix eigenvalue methods: eqs 4 and 9 can be compared with eqs 1 and 2.

Typically, about 50 000−150 000 Chebyshev iterations were required for each initial condition considered to adequately resolve the relevant resonance parameters. The calculations range in computational time from 1 to 3 days on a 667 MHz, Compaq XP1000 workstation using the parameter set J-4 in Table 1.

III. Results

A. Bound States. Relative to the bottom of the H_2O potential minimum, the energy of OH(v_{OH}=j_{OH}=0) + H is 44 726.9 cm^{-1} on the 1A′ surface of Ho et al.[3] Bound states have energy less than this threshold. [Subtracting out the zero-point energy of 4647.4 cm^{-1}, D_0(OH+H) = 40 079.5 cm^{-1}.] On the basis of several large-scale Lanczos determinations of the bound states, we estimate for $J = 0$ and even exchange H atom symmetry that there are 588 bound states. Table 1 lists the grid and basis set parameters for our most ambitious calculations, corresponding to Hamiltonian matrices ranging in dimension from 1.28×10^6 to 3.90×10^6. Table 2 lists selected energy levels from our best calculation, which corresponds to parameter set J-3 in Table 1. The root-mean-square deviations between all 588 energy levels from our best (J-3) calculation and the parameter sets R-1, J-1, and J-2 are 0.11, 0.06, and 0.01 cm^{-1}. The largest magnitude deviations of any single energy level from the R-1, J-1, and J-2 results with respect to the J-3 levels are 1.56, 1.37, and 0.27 cm^{-1}. We believe that our energy levels are converged to within 1 cm^{-1}, although it is still possible there could be some slightly larger uncertainty pertaining to the very highest two levels (which are associated with the largest magnitude deviations).

TABLE 2: Selected Energy Levels from the Present Calculations Compared with Those of Mussa and Tennyson (MT)[5,6]

	energy[a]/cm^{-1}		
level no.	present	MT	present − MT
518	43293.15	43293.23	−0.08
519	43326.78	43326.90	−0.12
520	43328.68	43328.71	−0.03
521	43344.85	43344.85	0.00
522	43354.04	43354.05	0.01
538	43752.09	43752.11	−0.02
539	43755.71	43755.73	−0.02
540	43776.08	43776.13	−0.05
541	43793.18	43793.33	−0.15
542	43808.98	43808.99	−0.01
558	44197.28	44197.26	0.02
559	44204.29	44204.42	−0.13
560	44210.83	44210.89	−0.06
561	44235.45	44235.47	−0.02
562	44258.64	44258.65	−0.01
568	44354.42	44354.47	−0.05
569	44372.75	44372.75	0.00
570	44404.41	44404.47	−0.06
571	44415.22	44415.24	−0.02
572	44433.11	44433.25	−0.14
578	44552.32	44552.42	−0.10
579	44559.94	44559.97	−0.03
580	44568.40	44568.43	−0.03
581	44575.40	44577.56	−2.16
582	44589.81	44589.94	−0.13
583	44649.15	44650.38	−1.23
584	44651.75	44658.61	−6.86
585	44666.96	44668.83	−1.87
586	44706.01	44710.32	−4.31
587	44720.70	44723.54	−2.84
588	44722.77		

[a] The energies are reported relative to the potential minimum of water as the zero of energy. (The zero-point energy of H_2O is 4647.43 cm^{-1}.)

Mussa and Tennyson (MT)[5,6] obtained accurate estimates of the first 580 levels. Table 2 compares our results with selected energy levels from their calculations. Our best results for the first 580 levels have a root-mean-square deviation of 0.08 cm^{-1} from the MT results, and the maximum absolute deviation for any one energy level is 0.65 cm^{-1}. This excellent level of agreement is reflected in Table 2. Also included in Table 2 are the remaining 7 bound states (581−587) obtained by MT. (The 588th state was found not have an energy below the threshold

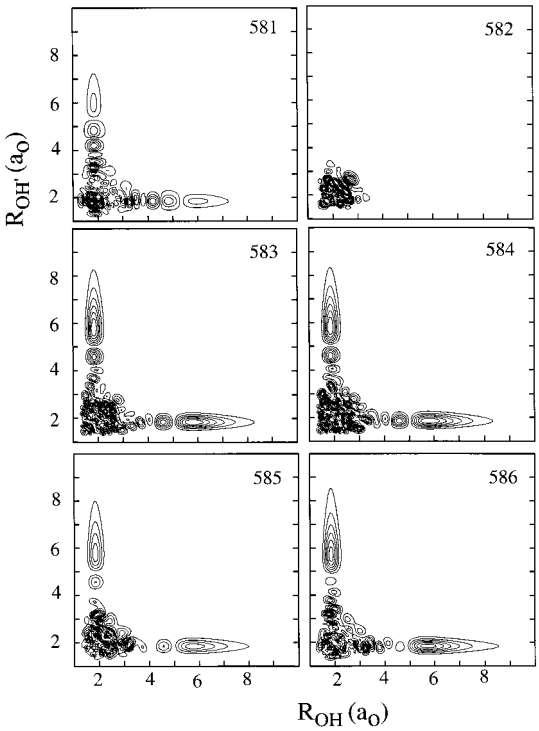

Figure 1. Contour maps of wave functions for states 581−586. The HOH bond angle has been fixed at $\theta = 105°$ to generate the contour maps.

in the MT calculations.) MT carried out careful convergence checks and concluded that these states were probably not well converged, and therefore it is not surprising that the present calculations can deviate by up to nearly 7 cm^{-1} from their results.

The highest bound states are particularly difficult to converge and are responsible for the necessity of large grids as in Table 1. Some insight into the reason for this is provided by an inspection of the eigenfunctions, ψ^n. It suffices to determine the eigenfunctions 581−586 at the J-1 parameter set level, since we find that each of these states is converged to better that 0.003 cm^{-1} with this parameter set. Figure 1 displays contour maps of the eigenfunctions for states 581−586 in terms of the two OH distances, R_{OH} and $R_{OH'}$, with the HOH angle, θ, fixed at 105°. (We use spline interpolation of the wave functions inferred with our Jacobi-based grids.) With the exception of state 582, one sees that quite large extensions in the two bond distances can occur. As we will see later in the case of the resonances, there can be angular variation in the wave functions. However, one can calculate the average value of the OH bond distance, $\langle R_{OH} \rangle$, and its associated standard deviation or spread, σ_{OH}, from each eigenstate including all coordinates and angles to verify that these states are extended. We find that state 582, as might be expected from Figure 1, is rather compact with ($\langle R_{OH} \rangle \pm \sigma_{OH}$) = 2.2 ± 0.5 a_0. States 581, 583, 584, 585, and 586 are indeed extended since all have $\langle R_{OH} \rangle$ ranging between 2.5 and 3.1 a_0, and spreads σ_{OH} ranging from 0.9 to 1.7 a_0. We can also decompose these wave functions into more tightly bonded and extended components. For the case of states 583 and 584, for example, contour maps associated with the simple superpositions $\psi^{\pm} = 2^{-1/2}(\psi^{583} \pm \psi^{584})$ are displayed in Figure 2. This type of decomposition is one means of deducing approximate, zero-order eigenstates that are mixed by some possible resonance interaction or perturbation. It has been used widely in intramolecular dynamics work, including of course the analysis of the local modes in water.[32−34] It is clear that one such superposition

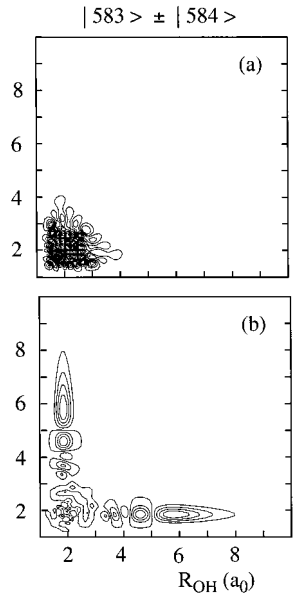

Figure 2. Contour maps ($\theta = 105°$) of $\psi^{\pm} = 2^{-1/2}(\psi^{583} \pm \psi^{584})$. Compare with states 583 and 584 in Figure 1.

(whether it is ψ^+ or ψ^- is immaterial and depends on phase conventions), shown in Figure 2a, is very localized in the interaction region whereas the other superposition state, shown in Figure 2b, corresponds to significant extension of the OH bonds. A similar interpretation can be made of states 585 and 586, although they are more energetically separated than states 583 and 584. (We assumed equal mixing of the eigenstates. Of course a variety of mixings could be considered to obtain the cleanest decomposition.)

States 587 and 588 are displayed in Figure 3, a and b. We employed our best parameter set, J-3, to compute these states because they can be even more extended than states 581−586. It is clear from the figure that state 587 is remarkably extended, with significant lobes centered near $R_{OH} = 9$ a_0. ($\langle R_{OH} \rangle = 5.3$ a_0 for this state.) State 588 is more tightly bound ($\langle R_{OH} \rangle = 5.0$ a_0), but does have some extended state character. States 587 and 588 lie within just 5 cm^{-1} of the OH + H threshold. It is conceivable that a more extensive calculation, with grid extents even beyond those in Table 1, might result in at least one of these states (or perhaps a superposition of these states) being in the resonance (above threshold) regime. We believe, however, because all the bound state parameter sets in Table 1 unambiguously yielded 588 levels that this is probably not the case. (The approximations to states 587 and 588 calculated at the smaller, J-1 grid level were actually quite similar in spirit to those in Figure 3, although the degree of mixing between the tightly bonded and extended parts was more even.) However, such near-threshold details are probably quite sensitive to minor variations in the potential and a more thorough investigation would be very interesting.

B. Resonance States. The Chebyshev iterations were carried out with the grid, basis set, and absorption details outlined in Table 1. The initial conditions for the Chebyshev iterations were taken from the eigenvectors above the dissociation threshold inferred from the J-1 Lanczos calculations, as outlined in section IIC. The somewhat larger, J-4 grid, including absorption, was used in the propagations. By choosing the "moderate" J-4 grid it is possible that some very extended resonances will not be adequately described. However, the J-4 grid allowed us to carry out numerous calculations of the resonances and their nature that would not have been easy to do with significantly larger grids.

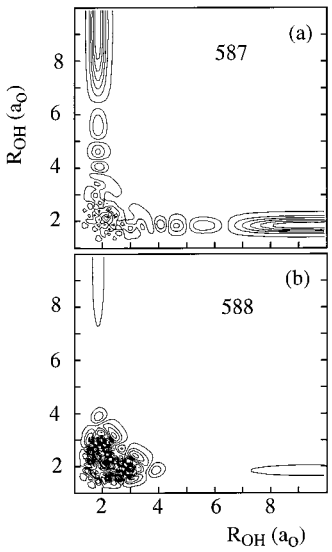

Figure 3. Contour maps ($\theta = 105°$) of eigenstates (a) 587 and (b) 588. The HOH bond angle has been fixed at 105°.

TABLE 3: Resonance Energies and Decay Widths[a]

resonance	energy/cm^{-1}	width/cm^{-1}
1	44739.9	0.38
2	44751.6	0.22
3	44761.6	0.075
4	44777.8	9.0
5	44794.6	0.50
6	44799.6	3.2
7	44815.6	2.9
8	44830.8	0.82
9	44832.0	5.3
10	44846.8	0.01
11	44867.8	0.47
12	44901.2	0.16
13	44932.2	8.0
14	44936.6	0.39

[a] The resonance energies are reported relative to the minimum potential energy of H_2O.

We focused on resonances within the first 250 cm^{-1} above threshold. In Table 3 we list energies and decay widths of the 14 resonance states that we identified. In addition to calculations with the absorption strength in Table 1, we also carried out calculations with half this strength to verify the robustness of the resonances. These results suggest that our resonance positions are probably accurate to within 1 cm^{-1}. The widths are more difficult to converge, and appear to be converged to within 20% with the exception of the very smallest and very largest widths which could be have slightly larger uncertainties. Figure 4 displays the energies and widths (solid circles) and, for comparison, a decay width based on RRKM theory ideas (solid line). The RRKM estimate is taken from the standard expression[35]

$$\Gamma_{RRKM} = \frac{N(E)}{2\pi\rho(E)} \tag{10}$$

where $N(E)$ is the sum of states at a transition state and $\rho(E)$ is the density of states associated with the reactants. The density $\rho(E)$ is inferred from our resonance energies (Table 3) to be 0.068 ± 0.003 states/cm^{-1}. To make this estimate, we constructed the sum of states for our resonances and fit the result to a line. The slope of the line is then ρ. (With only 14 resonances in the energy interval, it is not possible to determine with any accuracy an energy variation in the density. The value of ρ obtained does not differ substantially from comparable estimates of the actual bound state density just below the threshold.) Note that our resonance states all have even hydrogen atom exchange symmetry and so that the density pertains to just even states. Since the reaction is barrierless, $N(E)$ is taken to be the number of open OH vibration−rotation states (v_{OH}, j_{OH}) at energy E. To be consistent with the symmetry restriction of the reactant density, $N(E)$ is estimated based on just one of the two possible OH product channels. Over the first 250 cm^{-1} above threshold, just $v_{OH} = 0$ is open and only the first 4 j_{OH} can contribute to $N(E)$. With a few exceptions, the resonance decay widths in Figure 4 tend to be lower than the RRKM estimates. The average quantum resonance decay width is ≈2.2 cm^{-1}, which contrasts with the RRKM estimate ranging from 2.3 to 9.4 cm^{-1}. The energy regime in question corresponds to the limit of nonoverlapping resonances since the average energy spacing is $\rho^{-1} \approx 15$ cm^{-1}, i.e., 7 times larger than the average quantum decay width. Even in this nonstatistical limit one might have expected that the average quantum decay width would be in better agreement with the RRKM estimate.[36,37] However, a significant number of resonances have energy either trapped in the nonreactive bending mode and/or distributed between the two OH stretches, which probably leads to small decay widths. Our result here is also similar in spirit to results obtained for HOCl,[25] and HCO and HNO.[38] Of course another possible source for the discrepancy between our average decay width and simple RRKM theory is that we may not have found all the resonances with relatively large decay widths. Unfortunately, the proper description of very fast decaying resonances will presumably require calculations based on much larger grids (e.g., the J-3 parameter set of Table 1 or larger) because we expect such states to be very extended in character.

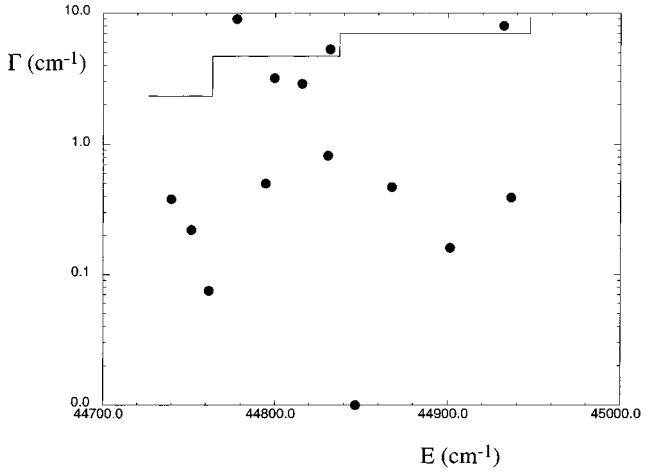

Figure 4. Resonance decay widths as a function of energy (relative to the bottom of the H_2O well), indicated as solid circles. An estimate of the decay width based on RRKM theory ideas is displayed as solid lines.

We now turn to a qualitative discussion of the nature of some of the resonance states listed in Table 3. The wave function for the lowest energy resonance (resonance 1 in Table 3) is depicted in Figure 5 at two different HOH bond angles, $\theta = 105°$ and 80°. Because this and most other resonance states exhibit a fairly high degree of bending excitation, angles that are smaller than the equilibrium bond angle for the water molecule (105°) can be important. The average value of θ for this resonance is 102°, and its spread is 41°, indicating significant bending excitation. (The spread in θ associated with no or little bending excitation is ≈20°.) In general, the wave functions are somewhat less compact at the smaller angles, probably because these geom-

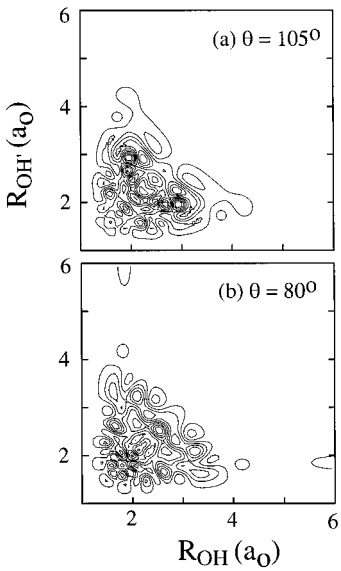

Figure 5. Contour maps of the first resonance ($E = 44\,739.9$ cm^{-1}, $\Gamma = 0.38$ cm^{-1}) wave function Table 3 at two different bond angles, (a) $\theta = 105°$ and (b) $\theta = 80°$.

etries are more conducive to the dissociation of an H atom. The striking aspect of resonance 1, however, is how compact it is, particularly in comparison with some of the highest excited bound states in Figures 1−3. We suspect that the continuum regime analogues of the spread out bound states will be fast-decaying resonances that are both difficult to stabilize theoretically and to observe experimentally. Resonances 4 and 13 in Table 3, we have verified, do tend to have significant extended character *and* they are the shortest lived resonances we have found. (They are also probably the least well converged regarding grid details.).

There are some resonance states that we find particularly interesting. The one "hyperspherical"[16] resonance that we found is resonance 5. (A hyperspherical state is one that would be best assigned in terms of a polar coordinate system based on the two bond distances).[16] Figure 6a−c shows contours of the wave function with θ fixed at 105°, 80°, and 60°, respectively. (The average value of θ for this resonance is 94°, and its spread is 31°.) What is most interesting here is that at angles near the equilibrium bond angle of water, this can be characterized as a "square state" or as a state with both hyperspherical and local mode character. At the smaller angles, however, resonance 5 is nearly a pure hyperspherical state.

A particularly interesting local mode resonance, resonance 7, was found and it is depicted in Figure 7a. This state, like all previous resonance and bound states discussed so far, arose from an even H atom exchange calculation. It is a straightforward matter to carry out additional, odd H atom exchange calculations and locate the companion resonance for this state, which is shown in Figure 7b. Addition and subtraction[33,34] of these two symmetry states yields the pure local mode excitations in question—displayed in Figure 7, c and d. While a little difficult to see, this local mode excitation corresponds to 14 quanta (nodes) along one OH bond and, more clearly, one quantum of excitation in the other OH bond. Whereas most of the resonances we have found have significant spreads in θ and complicated nodal patterns when plotted in terms of θ, this resonance was found to be mostly a zero-point bending state.

IV. Concluding Remarks

We hope that these calculations of the high-lying bound states and resonance states of water will stimulate further research. It would be especially gratifying if some resonances near threshold were found experimentally. Of course, it is doubtful that the specific resonances we found will actually be present at the corresponding experimental excitation energies. While the potential employed was based on accurate ab initio data,[3] it is not of "spectroscopic" accuracy. On the other hand, being a global surface, it should describe the dissociation process reasonably well. We therefore believe our results are indicative of the type of resonances (and bound states) that will exist near

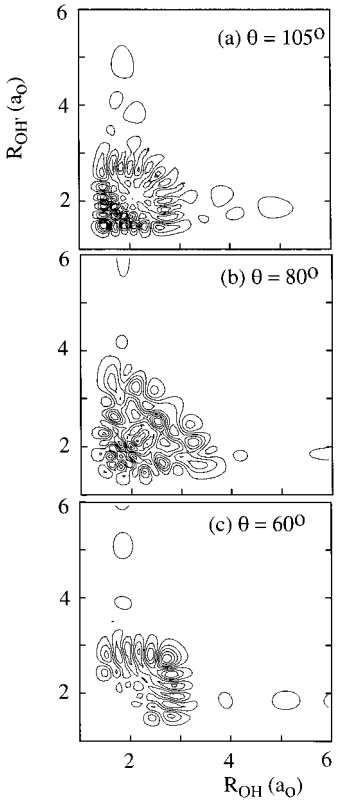

Figure 6. Contour maps of the fifth resonance ($E = 44\,794.6$ cm^{-1}, $\Gamma = 0.50$ cm^{-1}) wave function Table 3 at three different bond angles, (a) $\theta = 105°$ and (b)) $\theta = 80°$ and (c) $\theta = 60°$.

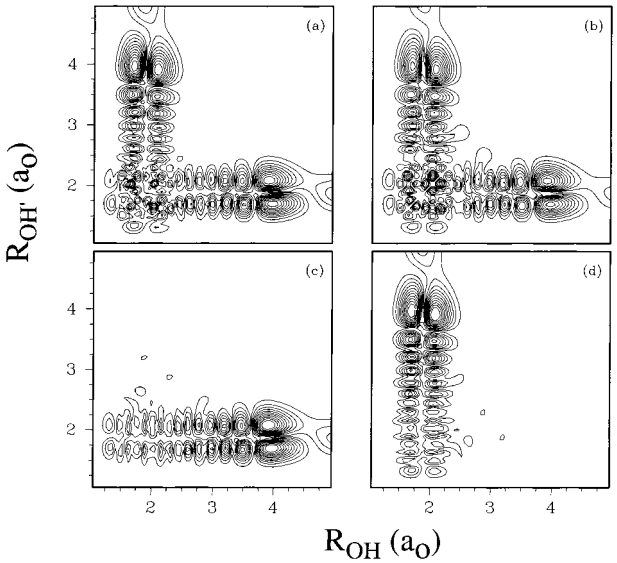

Figure 7. Contour maps ($\theta = 105°$) of the 7th resonance state ($E = 44\,815.6$ cm^{-1}, $\Gamma = 2.9$ cm^{-1}) are displayed in panel a. Panel b shows a similar state obtained from a calculation corresponding to odd H atom exchange symmetry. The sum and difference of the states in (a) and (b) are depicted in panels c and d.

threshold. Also useful would be more theoretical work to map out the possible spectroscopic pathways, in terms of transitions through intermediate states, that would permit experimentalists to access such resonances. Finally, more work needs to be done to fully understand the threshold region, in particular to see if there are additional, faster decaying resonances.

Acknowledgment. S.K.G. was supported by the Office of Basic Energy Sciences, Division of Chemical Sciences, U.S. Department of Energy, under Contract No. W-31-109-ENG-38. E.M.G. acknowledges support for this research from NSF grant CHE-9970994. We thank C. Wittig for providing essential motivation and R. W. Field for useful comments.

References and Notes

(1) Barnes, R. J.; Gross, A. F.; Sinha, A. *J. Chem. Phys.* **1997**, *106*, 1284.
(2) Wittig, C., private communciation.
(3) Ho, T.-S.; Hollebeek, T.; Rabitz, H.; Harding, L. B.; Schatz, G. C. *J. Chem. Phys*. **1996**, *105*, 10472.
(4) Csaszar, A. G.; Mills, I. M. *Spectrochim. Acta, Part A* **1997**, *53*, 1101.
(5) Mussa, H. Y.; Tennyson, J. *J. Chem. Phys.* **1999**, *109*, 10885.
(6) AIP Document No. EPAPA: E-JCPSA6-109-025848 contains all the energy levels calculated by Mussa and Tennyson and can be retrieved from http://www.aip.org/epaps/epaps.html.
(7) Choi, S. E.; Light, J. C. *J. Chem. Phys*. **1992**, *97*, 7031.
(8) Bramley, M. J.; Carrington, T., Jr. *J. Chem. Phys.* **1993**, *99*, 8519.
(9) Huang, S.-W.; Carrington, Jr., T. *Chem. Phys. Lett.* **1999**, *312*, 311.
(10) Cullum, J.; Willougbhy, R. A. *J. Comput. Phys.* **1981**, *44*, 329.
(11) Trefethen, L. N.; Bau, D. *Numerical Linear Algebra*; SIAM: Philadelphia, PA, 1997.
(12) Mandelshtam, V. A.; Taylor, H. S. *J. Chem. Phys.* **1995**, *103*, 2903.
(13) Grozdanov, T. P.; Mandelshtam, V. A.; Taylor, H. S. *J. Chem. Phys*. **1995**, *103*, 7990.
(14) V. A. Mandelshtam, V. A.; Taylor, H. S. *J. Chem. Phys.* **1997**, *107*, 6756.
(15) Gray, S. K.; Balint-Kurti, G. G. *J. Chem. Phys*. **1998**, *108*, 950.
(16) Hartke, B.; Janza, A. E.; Karrlein, W.; Manz, J.; Mohan, V.; Schreier, H.-J. *J. Chem. Phys.* **1992**, *96*, 3569.
(17) Bacic, Z.; Light, J. C. *Annu. Rev. Phys. Chem*. **1989**, *40*, 469.
(18) Light, J. C.; Hamilton, I. P.;. Lill, J. C. *J. Chem. Phys.* **1985**, *82*, 1400.
(19) Skokov, S.; Qi, J.; Bowman, J. M.; Yang, C.-Y.; Gray, S. K.; Peterson, K. A.; Mandelshtam, V. A. *J. Chem. Phys*. **1998**, *109*, 10273.
(20) Chen, R.; Guo, H. *J. Comput. Phys*. **1997**, *136*, 494.
(21) Chen, R.; Guo H. *Chem. Phys. Lett.* **1999**, *308*, 123.
(22) Huang, S.-W.; Carrington, T., Jr. *J. Chem. Phys.* **2000**, *112*, 8765.
(23) Johnson, B. R.; Reinhardt, W. P. *J. Chem. Phys*. **1986**, *85*, 4538.
(24) Jolicard, G.; Leforestier, C.; Austin, E. J. *J. Chem. Phys.* **1988**, *88*, 1026.
(25) Skokov, S.; J. M. Bowman, J. M. *J. Chem. Phys.* **1999**, *111*, 4933.
(26) Taylor, H. S. *Adv. Chem. Phys.* **1970**, *18*, 91.
(27) Bisseling, R. H.; Kosloff, K.; Manz, J. *J. Chem. Phys.* **1985**, *83*, 993.
(28) Gray, S. K. *J. Chem. Phys.* **1992**, *96*, 6543.
(29) Wall, M. R.; Neuhauser, D. *J. Chem. Phys.* **1995**, *102*, 8011.
(30) Marple, S. L., Jr. *Digital Spectral Analysis with Applications*; Prentice Hall: Englewood Cliffs, NJ, 1987.
(31) Engel, V. *Chem. Phys. Lett.* **1992**, *189*, 76.
(32) Lawton, R. T.; Child, M. S. *Mol. Phys.* **1980**, *40*, 773.
(33) Lawton, R. T.; Child, M. S. *Mol. Phys.* **1981**, *44*, 709.
(34) Sibert, E. L., III; Hynes, J. T.; Reinhardt, W. P. *J. Chem. Phys*. **1982**, *77*, 3595.
(35) Baer, T.; Hase, W. L. *Unimolecular Reaction Dynamics: Theory and Experiments*; Oxford University Press: New York, 1996.
(36) Waite, B. A.; Miller, W. H. *J. Chem. Phys.* **1980**, *73*, 3713.
(37) Peskin, U.; Reisler, H.; Miller, W. H. *J. Chem. Phys.* **1994**, *101*, 9672.
(38) Stumpf, M.; Dobbyn, A. J.; Mordaunt, D. H.; Keller, H.-M.; Fluethmann, H.; Schinke, R.; Werner, H.-J.; Yamashita, K. *Faraday Discuss.* **1995**, *102*, 193.